Impact of Voltage Unbalance System on Modern Microgrid System under High Penetration of Fast Charging Station

Noppanut Chitgreeyan[1], Yuttana. Kongjeen[1], Krittidet Buayai[1,*], and Kaan Kerdchuen[1]

ARTICLE INFO

Article history:
Received: 25 May 2020
Revised: 31 July 2020
Accepted: 1 September 2020

Keywords:
Backward-forward sweep
Fast-charging station
Microgrid
Total power loss
Unbalanced power flow
Voltage unbalance

ABSTRACT

This paper presents the analysis of unbalanced load power flow and impact from high penetration of fast charging stations connected to a modern microgrid system. A modification of the backward-forward sweep method was applied to solve the unbalanced power flow of the grid. A fast-charging station (FCS) was represented in a three-phase balanced system by using a voltage-dependent model. The IEEE 37 bus test system was selected to analyze the problem for the purpose. The scenario for analyzing the impact of FCS was defined in nine cases with 50kW per station on each bus. The results showed that the penetration level of FCS on each bus impact on the total power loss was more than the voltage unbalance factor (VUF). Significantly, case 3C had a penetration level of FCS of 24.42%, and the percentage difference of total power loss was 74.8265%, while the percentage difference of Max.VUF was 17.1579%. Therefore, the influence of total power loss had more impact than voltage unbalance when FCS was installed on the three-phase balanced system.

1. INTRODUCTION

Nowadays, an electrical power system is connected by a new modern load that can be moved to each area of the grid for consuming the electric power. This new modern load is called an electric vehicle (EVs) [1]. The role EVs is a high potential in many sectors for managing the energy of the grid. The benefit of EVs is related to the lowest impact on the environment when compared with the traditional car [2]. Nowadays, EVs have increased in every country because the governments promote and give incentives to change the traditional car to EVs. Therefore, EVs are becoming an essential load of the grid because they need electricity to move with the battery energy storage pack (BESP). The BESP is connected to a battery charger by an electric cable for charging the battery. The charger consumes energy from the grid when EVs are connected to charge the battery. The power for charging the battery differs depending on the size of the battery and the type of charger used. A high impact charging type into the grid is called a fast- charging station (FCS) [3]. Many researchers have revealed the increased effect of FCS in terms of low power oscillation, high energy demand and many problems to the grid [4, 5].

Therefore, the purpose of this paper is to study the effect of the FCS on the microgrid under unbalanced conditions using unbalanced power flow analysis. The voltage-dependent model of the FCS load was represented by defining a three phase balanced system. The FCS is connected to the grid in different positions of the microgrid.

The rest of this paper is organized as follows: Section 2 purposes the methodology consisting of the unbalanced power flow; FCS mathematical model, total power loss, and voltage unbalance factor (VUF), mean absolute percentage error (MAPE) and scenarios for simulation, respectively. Simulation results are presented in Section 3. Meanwhile, Section 4 shows the conclusion and discussion.

2. METHODOLOGY

The FCS was defined with a three phase balanced system at 50 kW per station by using level 4 on a commercial location [1]. Theories related to the impact analysis of electric vehicles can be presented as follows.

2.1 Unbalanced power flow (UPF)

The Radial distribution system (RDS) was used to solve the power flow with UPF conditions. The branch reordering used to arrange the branch number ($\mathbf{B_x}$) from the root node to the end of node by relating the branch number ($\mathbf{B_x}$) between the node ($\mathbf{N_x^t}$) and to the node ($\mathbf{N_x^f}$) as equation (1) and as shown in Fig.1. Meanwhile, equation (2) was defined as the node condition with the same

[1]*Department of Electrical engineering, Faculty of Engineering and Architecture, Rajamangala University of Technology Isan, Nakhonratchasima, Thailand.*

**Corresponding author:* Krittidet Buayai; Phone: +66-44-233-000; E-mail: kittavit.bu@rmuti.ac.th.

number of the node and not equal to one. Equation (3) was used to find the next branch matrix, in the state of the node, not the same previous $\mathbf{Node^{(k)}}$ matrix. This paper uses a three-phase with the four wires system for solving the problem of the purpose, as described in Fig.2.

$$\left[\mathbf{Branch^{(k)}}\right] = \begin{bmatrix} \mathbf{B_1} & \mathbf{N_1^f} & \mathbf{N_1^t} \\ \mathbf{B_2} & \mathbf{N_2^f} & \mathbf{N_2^t} \\ \vdots & \vdots & \vdots \\ \mathbf{B_n} & \mathbf{N_n^f} & \mathbf{N_n^t} \end{bmatrix} \tag{1}$$

$$\left[\mathbf{Node^{(k)}}\right] = \mathbf{N_i^t} \qquad \mathbf{;i = 1:n, N^t \neq N^f, N^f \neq 1} \tag{2}$$

$$\left[\mathbf{Branch^{(k+1)}}\right] = \left[\mathbf{Branch^{(k)}}\right] \qquad \mathbf{;N^t \neq \left[Node^{(k)}\right]} \tag{3}$$

where $\mathbf{B_x}$ represents branch number; $\mathbf{N_x^f}$ and $\mathbf{N_x^t}$ represents a branch from the node to the node that connected between the nodes ($\mathbf{Node^{(k)}}$); **n** represents the total number of buses in the network.

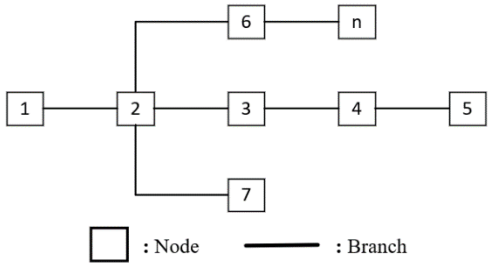

Fig. 1: Node numbering methodology.

Fig. 2 shows the transmission line connected between a *Node(i-1)* and *a Node(i)* by representing three-phase with four wires. The three phase transmission line model used to solve from the purpose.

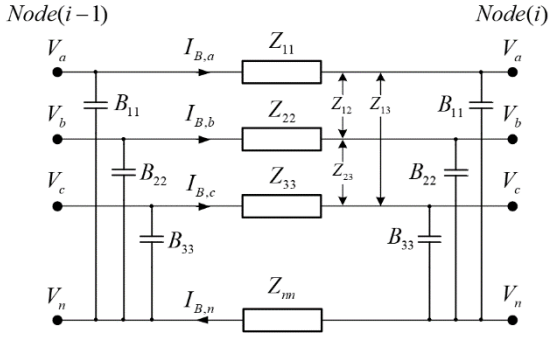

Fig. 2: Three phase transmission line model [7].

where $I_{B,x}$ represents current flow from *Node(i-1)* to *Node(i)* of each phase; V_x represents phase voltage of each phase; B_x represents the susceptance of the transmission line; Z_{xx} represents an impedance of the transmission line. The B_x and Z_{xx} defined in a matrix form as (4) and (5) as follows.

$$\left[Z_{Line}\right] = \begin{bmatrix} Z_{11} & Z_{12} & Z_{13} \\ Z_{21} & Z_{22} & Z_{23} \\ Z_{31} & Z_{32} & Z_{33} \end{bmatrix} \tag{4}$$

$$\left[B_{Line}\right] = \begin{bmatrix} B_{11} & B_{12} & B_{13} \\ B_{21} & B_{22} & B_{23} \\ B_{31} & B_{32} & B_{33} \end{bmatrix} \tag{5}$$

Backward sweep (BS) was applied to a Kirchhoff current law to solve an unbalanced power flow by using data from the reordering process. The BS found the current of each branch backward from the end of the root of the node. All branch current flows ($I_{B,x}$) were combined with returned current flow in the neutron transmission line ($I_{N,x}$) and phase line as (6) and (7), respectively. Therefore, the total current flow of the network can be represented by (8) and (9).

$$I_{N,x}(i) = \left(\frac{P_x(i) + jQ_x(i)}{V_x(i)}\right)^* + j \cdot B(i) \cdot V_x(i) \tag{6}$$

$$\begin{bmatrix} I_{N,a} \\ I_{N,b} \\ I_{N,c} \end{bmatrix} = \begin{bmatrix} \left(\frac{P_a + jQ_a}{V_a}\right)^* \\ \left(\frac{P_b + jQ_b}{V_b}\right)^* \\ \left(\frac{P_c + jQ_c}{V_c}\right)^* \end{bmatrix} + j \cdot \left[B_{Line}^{abc}\right] \cdot \begin{bmatrix} V_a \\ V_b \\ V_c \end{bmatrix} \tag{7}$$

$$I_{B,x} = I_{N,x} + \sum_{i=1}^{3} I_{B,x}(m) \tag{8}$$

$$\begin{bmatrix} I_{B,a} \\ I_{B,b} \\ I_{B,c} \end{bmatrix} = \begin{bmatrix} I_{N,a} \\ I_{N,b} \\ I_{N,c} \end{bmatrix} + \begin{bmatrix} \sum_{m \in M} I_{B,a}(m) \\ \sum_{m \in M} I_{B,b}(m) \\ \sum_{m \in M} I_{B,c}(m) \end{bmatrix} \tag{9}$$

where *x* represents the number of transmission lines; $I_{B,x}$ represents branch current connected to node (*m*).

Forward sweep (FS) was applied to find voltages node ($V_x(i)$) by using current flow, and impedance of the transmission line ($Z_{line}(i)$) from the root node to the end of a node can be described as (10) and (11) as follows [2].

$$V_y(i) = V_y(i-1) - I_{B,y}(i) \cdot Z_{Line}(i) \tag{10}$$

$$\begin{bmatrix} V_a(i) \\ V_b(i) \\ V_c(i) \end{bmatrix} = \begin{bmatrix} V_a(i-1) \\ V_b(i-1) \\ V_c(i-1) \end{bmatrix} - \left[Z_{Line}^{abc} \right] \cdot \begin{bmatrix} I_{B,a}(i) \\ I_{B,b}(i) \\ I_{B,c}(i) \end{bmatrix} \quad (11)$$

where *y* represents number of nodes; *i* is the number of transmission lines from the reordering process.

The change in complex voltage $\left(\Delta V_j^k\right)$ from the backward-forward sweep iteration (*k*) then can be expressed by (12) and (13) within tolerance limit (ε).

$$\Delta V_j^{(k)} = V_j^{(k)} - V_j^{(k-1)} \quad (12)$$

$$\left\{ \begin{array}{c} \left| \mathrm{Re}\left(\Delta V_j^{(k)}\right) \right| \le \varepsilon \\ \left| \mathrm{Im}\left(\Delta V_j^{(k)}\right) \right| \le \varepsilon \\ \left| \Delta V_j^{(k)} \right| \le \varepsilon \end{array} \right\} \quad (13)$$

2.2 *Load modeling in the electrical power system*

A load model relates the voltage magnitude of frequency based on algebraic function to any instant of time. Moreover, the load model reveals the characteristics of the active power component (P_L) and reactive power component (Q_L) at any instant of time. Traditionally, the load characteristics at any bus (*i*) are represented by the voltage dependency with the exponential model as follows [8].

$$P_{L_i} = P_{L_{i0}} \left(\frac{V_i}{V_{i0}} \right)^{n_{pi}} \quad (14)$$

$$Q_{L_i} = Q_{L_{i0}} \left(\frac{V_i}{V_{i0}} \right)^{n_{qi}} \quad (15)$$

where *i* represents number of PQ buses; $P_{L_{i0}}$ and $Q_{L_{i0}}$ define the nominal active power and reactive power, respectively; P_{L_i} and Q_{L_i} define active and reactive power components of the load when the bus voltage magnitude (V_i) vary from the nominal voltage; n_{pi} and n_{qi} define the load indices as constant power $\left(n_{pi} = n_{qi} = 0\right)$, constant current $\left(n_{pi} = n_{qi} = 1\right)$, and constant impedance $\left(n_{pi} = n_{qi} = 2\right)$, respectively.

The FCS was defined with a three-phase balanced system at 50 kW per station by using the three levels converter of DC fast charging. The topology of the FCS connected to the grid was combined with a power transformer, AC to DC rectifier, DC to DC converter and battery for energy storage of the EV can be presented in Fig. 3 as follows [4].

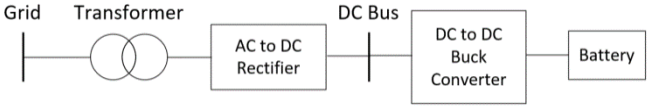

Fig. 3: Block diagram of the FCS [4].

Fig.3 shows the block diagram of the EV connected to the grid when charging the EV in the FCS. The electricity from the grid was transferred throughout the step-down transformer to the charging control unit (AC-DC rectifier and DC-DC converter). Then, the EV was represented by the battery. FCS load characteristics were dependent on the electrical power rate of the charger and level of state of charge (SOC), the energy storage for charging the battery. Voltage-dependent load (VDL) was represented in the FCS as described by [4,9]. They consisted of constant power (*b*) and voltage-dependent (*a*) component by relating voltage magnitude.

$$P_{EVi} = P_{0i} \left(b + a \left(\frac{V_i}{V_{0i}} \right)^{\alpha} \right) \quad (16)$$

$$Q_{EVi} = P_{EVi} \times \tan\left(\theta_i\right) \quad (17)$$

where P_{EVi}, Q_{EVi} are active power and reactive power of FCS, respectively; θ_i is a power factor angle of FCS and 0.97 is the given power factor; V_{0i} is the nominal voltage, and V_i is the variable voltage on a battery charging process. α is the exponential indices of charging characteristics given as -3.107; *i* is the number of PQ buses; P_{0i} is the nominal active power. Meanwhile, constant power and voltage-dependent were defined as 0.93 and 0.03, respectively.

2.3 Total power loss

The RDS for testing the system has a connected load traditionally, and there were different voltage profiles affected by the load. The total power loss is an important key to investigate the RDS because the load increases conditions that directly affect the total power loss of the electrical power system. Equation (18) shows the active power loss of branches ($P_{Loss,x}$) of a three-phase that was delivered from the current flows ($I_{B,x}$) and branch impedances. Therefore, the total power loss of the RDS is computed by summing each current flow of branch (*n*) on each phase as (19).

$$P_{Loss,x} = \mathrm{Real}(I_{B,x}^2(i) \cdot Z_{Line}(i)) \quad (18)$$

$$Total\ P_{Loss} = \sum_{x=1}^{3} \sum_{i=1}^{n} \mathrm{Real}(I_{B,x}^2(i) \cdot Z_x(i)) \quad (19)$$

where $P_{loss,x}$ represents the active power loss of branch from the phase x; n and i represent the total number of branches; x is defined as the number of phases; Z_{line} and Z_x are the impedance of the branch transmission lines and transmission line from the phase x.

2.4 Voltage unbalance factor (VUF)

Generally, the RDS is in an unbalanced condition because most customers connect to a single-phase load. Therefore, the VUF is needed to evaluate planning load connection in the future. The VUF was delivered from the ratio of negative (V_2) and positive sequence (V_1) as equation (22) or using β coefficient from the line to line voltage as Equation (23) [10]. Furthermore, the ratios of maximum and average VUF were used to investigate the impact of the VUF from each node, as shown in (24) [10].

$$\begin{bmatrix} V_+ \\ V_- \\ V_0 \end{bmatrix} = \frac{1}{\sqrt{3}} \begin{bmatrix} 1 & a & a^2 \\ 1 & a^2 & a \\ 1 & 1 & 1 \end{bmatrix} \begin{bmatrix} V_a \\ V_b \\ V_c \end{bmatrix} \tag{20}$$

$$VUF(\%) = \sqrt{\frac{|V_-|^2 + |V_0|^2}{|V_+|}} \times 100 \tag{21}$$

$$VUF(\%) = \frac{V_2}{V_1} \times 100 \approx \sqrt{\frac{1-\sqrt{3-\beta}}{1+\sqrt{3-\beta}}} \tag{22}$$

$$\beta = \frac{V_{ab}{}^4 + V_{bc}{}^4 + V_{ac}{}^4}{\left(V_{ab}{}^2 + V_{bc}{}^2 + V_{ac}{}^2\right)^2} \tag{23}$$

$$Ratio = \frac{VUF_{\max}}{VUF_{\text{mean}}} \tag{24}$$

VUF regulations and standard limits are many; defined from each standard such as EN 50160, EN 61000, ANSI C84.1, IEEE Std 241-1990, IEEE Std 1159, NEMA MG-1 and IEC 61000-2-4. In summary, the VUF does not exceed the range between 1 - 3% [11-15]. Therefore, the lowest VUF is needed to maintain and analyze the solution for each load connected to the grid. VUF affects the power quality in the severe case of the rotating machine.

2.5 Mean absolute percentage error (MAPE)

The MAPE was adapted to solve the impact of FCS under an unbalanced power flow. The difference from the base case and each scenario were difficult discussed from the purpose. The MAPE needs to be minimal and close to zero that it explained a little data change. This paper was using MAPE to solve the data of the VUF base case and VUF from testing scenarios as (25) [16].

$$MAPE(\%) = \frac{1}{n} \times \sum_{t=1}^{n} \left| \frac{A_t - F_t}{A_t} \right| \times 100 \tag{25}$$

where A_t represents the base case; F_t describes data from the test case; n expresses the number of test data.

2.6 Penetration level of the FCS on the grid

Many loads connected to the grid were a significant problem in increasing the total power loss and low static voltage stability. The FCS had a crucial impact on the grid and it controlled the number and capacity of the charger. The penetration level of the FCS was used to evaluate the total number of the FCS by using the active power condition and can be expressed by (26) as follows [10].

$$Penetration\ Level(\%) = \frac{\sum_{i=1}^{N_{PEV}} P_{PEV}(i)}{\sum_{n=1}^{N_{Load}} P_{Load}(n)} \times 100 \tag{26}$$

are N_{PEV} and N_{Load} represent the number of FCS and loads connected to the grid; P_{PEV} and P_{Load} are active power of the FCS and each load type.

3. SIMULATION AND RESULTS

The IEEE 37 bus test system was used to analyze the impact of FCS into the microgrid from the purpose as Fig.4.

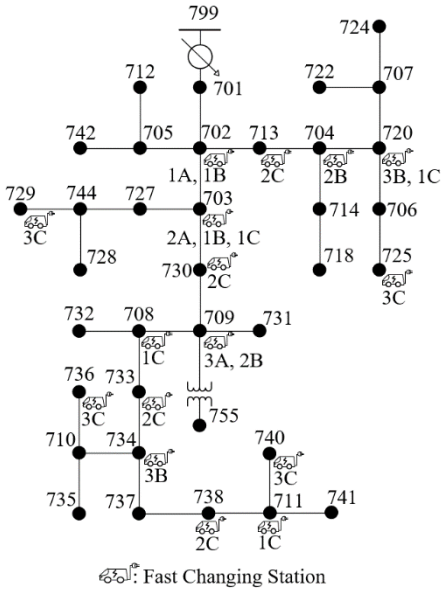

Fig. 4: IEEE 37 bus connected with FCS.

The impact of FCS was measured by defining the FCS installed on each location of the IEEE 37 node as Fig.4.

The IEEE 37 node ignored the auto voltage regulation on node No.799 and transformer disconnection on node No.755. The FCS rated 50 kW was the initial number of stations of 1, 2 and 4, respectively. The EV station position was defined by using randomly installed nodes in three categories as A, B and C. The scenarios for simulation can be divided into nine cases from Table 1 as follows.

Table 1: Scenarios to analyze the impact of FCS

Case	EV Station Position (Bus Number)	EV Sizing (kW)/Slot	Total EV Sizing (kW)
1A	702	50	50
2A	703	50	50
3A	709	50	50
1B	702, 703	50	100
2B	704, 709	50	100
3B	720, 734	50	100
1C	703, 708, 711, 720	50	200
2C	713, 730, 733, 738	50	200
3C	725, 729, 736, 740	50	200

The impact of FCS was shown in each scenario by comparing between the base case and each installed FCS. The %VUF profiles were selected to investigate the influences of FCS on the unbalanced power flow as follows.

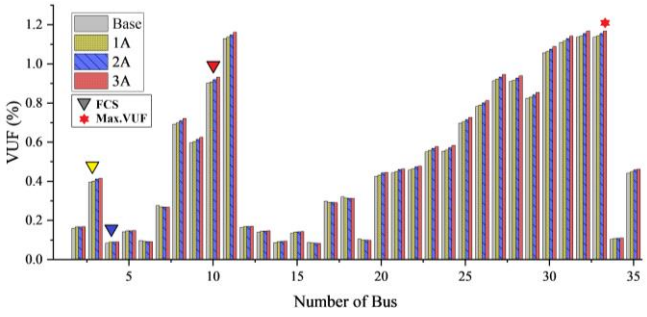

Fig. 5: Percentage of VUF profiles case 1A, 2A and 3A (50 kW).

Fig.5 shows the % VUF profiles of the FCS rated 50 kW, case 1A, case 2A and case 3A revealed the highest % VUF. Case 3A; at node No.33 remained at about 1.1678 %. These scenarios need to investigate the light load of the FCS installed near the root node or the energy source of the grid.

Fig. 6 shows the % VUF profiles of the FCS rated 100 kW, case 1B, case 2B, and case 3B revealed the highest the % VUF, Case 3B at the node No.33 remained at about 1.2010 %. So, increasing the number of FCS affected the % VUF. However, the Max. % VUF was the bus positions same as the previous case.

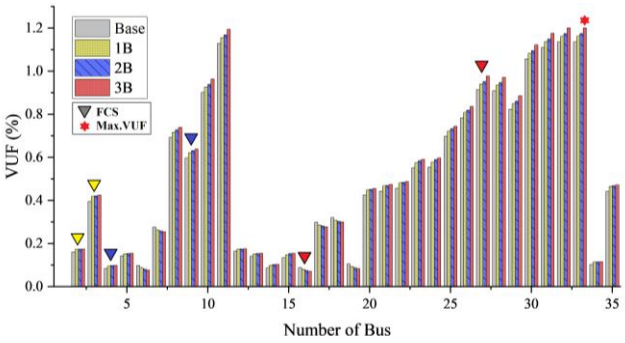

Fig. 6: Percentage of VUF profiles case 1B, 2B and 3B (100 kW).

Fig. 7 shows the % VUF profiles of the FCS rated 200 kW, case 1C, case 2C, and case 3C showed the highest % VUF. Case 3C; at node No. 32 remained at about 1.3315 %. Hence, the Maximum percentage of VUF changed from node No.33 to node No.32 due to the high penetration and distribution of FCS.

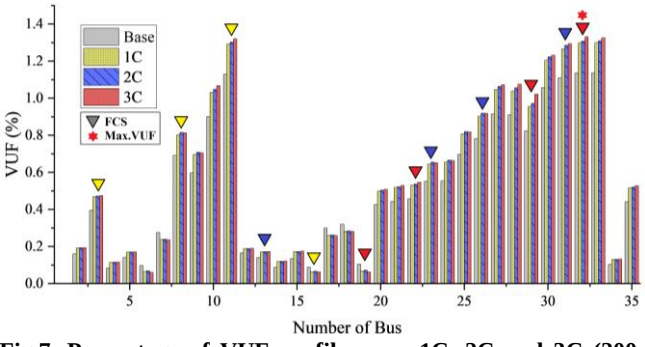

Fig.7. Percentage of VUF profiles case 1C, 2C and 3C (200 kW).

However, the percentage of the VUF was a small increase from the simulation results and within the VUF standard. The % VUF profiles are difficult to analyze because of the impact of the loads on the RDS. Therefore, the total power losses, the VUF and the MAPE were adapted to investigate the effect of the voltage unbalance system when connected to the FCS as Table 2.

Table 2 shows the simulation results of the total power loss, the percentage Max.VUF, and the rate of MAPE from each scenario. The penetration level of the FCS was defined by 6.1050 % for a rated 50 kW station, 12.2100% for a rated 100 kW station and 24.4200 % for a rated 200 kW station. So, the total power loss of the grid is presented by increasing from the base case of 42.2667 kW, the highest from categories A of 47.6500 kW (Case 3A), the highest from categories B of 54.3080 kW (Case 3B) and the highest from categories C of 73.8934 kW (Case 3A).

The percentage of VUF was used to investigate the voltage unbalance by defining the maximum value of the

Table 2: Simulation results from each scenario

Case	Total Ploss (kW)	Difference of Ploss (%)	Penetration Level (%)	Max.VUF (%)	Difference of Max.VUF (%)	Ratio of VUF	MAPE (%)
Base case	42.2667	0	0	1.1365	0	2.2900	-
Case 1A (50kW)	43.9651	4.0183	6.1050	1.1436	0.6247	2.2854	2.1897
Case 2A (50kW)	45.5882	7.8584	6.1050	1.1553	1.6542	2.2798	3.3790
Case 3A (50kW)	47.6500	12.7365	6.1050	1.1678	2.7540	2.2799	4.4097
Case 1B (100kW)	47.4307	12.2177	12.2100	1.1625	2.2877	2.2751	5.5933
Case 2B (100kW)	50.7186	19.9966	12.2100	1.1748	3.3700	2.2775	7.4977
Case 3B (100kW)	54.3080	28.4889	12.2100	1.2010	5.6753	2.2903	9.2181
Case 1C (200kW)	68.0898	61.0956	24.4200	1.2995	14.3422	2.3068	19.2058
Case 2C (200kW)	69.4502	64.3142	24.4200	1.3096	15.2309	2.2949	19.8944
Case 3C (200kW)	73.8934	**74.8265**	24.4200	1.3315	**17.1579**	2.3152	21.4138

VUF of each node. The maximum amount of Max.VUF (%) value from the base case was selected to compare the variant Max.VUF (%) value of each scenario. Interestingly, Max.VUF (%) value from the base case remained about 1.1365 %. It means that the original loads installed in the system were unbalanced. The categories A showed the highest Max.VUF (%) value of 1.1625 % (case 3A) with the difference Max. VUF (%) of 2.7540%. The categories B showed the highest Max.VUF (%) value of 1.2010 % (case 3B) with the difference Max. VUF (%) of 5.6753 %. The categories C showed the highest Max.VUF (%) value of 1.3315% (case 3C) with the difference Max. VUF (%) of 17.1579 %. The Ratio of VUF considered was used to analyze the variation in the ratio between the maximum value and the average value. It showed the lowest variants and closest to the values from the base case. The maximum ratio of VUF obtained from the case 3C was 2.3152, and the minimum ratio from the case 1B was 2.2751. Therefore, these values were not used to determine or evaluate the impact of the unbalanced system.

The MAPE percentage was used to investigate the changing rate of VUF from base case and each scenario. It means that each scenario was variant and changing. Therefore, category A showed the highest value of the MAPE (%) at 4.4097% (case 3A). Category B showed the highest amount of MAPE (%) at 9.2181 % (case 3B). Category C showed the highest value of MAPE (%) value at 21.4138 % (case 3C). By the result, the MAPE

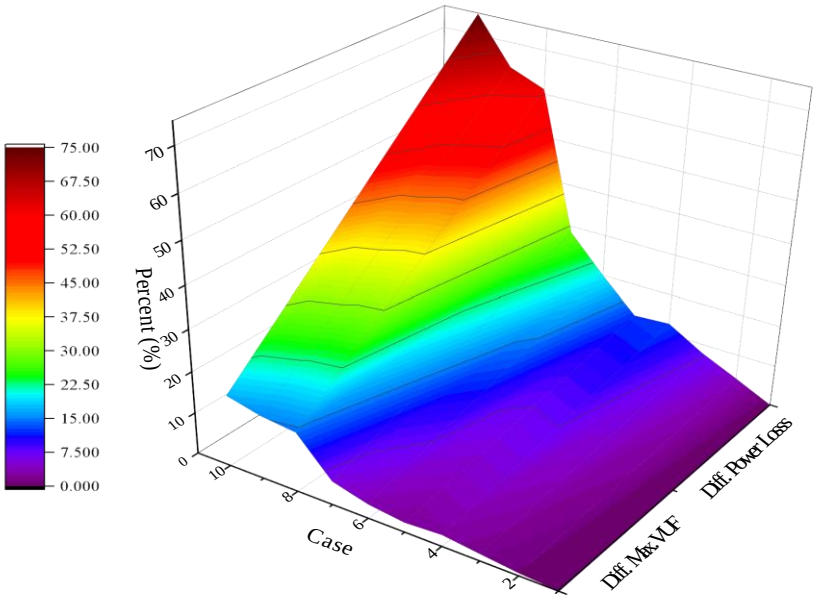

Fig. 8: The contour of the percentage difference the total power loss and difference Max.VUF.

percentage was close to the percentage difference of the Max.VUF. Therefore, the MAPE percentage can be used as a representation of the rate of the difference of VUF, however, considering the total active power loss and the Maximum percentage difference of VUF, the results revealed that the influence of the total power loss had more impact on the grid than the VUF. Significantly, the Case 3C (based on base case) showed the difference of Ploss (%) of 74.8265 %, when compared to the difference of Max. VUF (%) of 17.1579 %.

Fig.8 shows the comparison between the contour of power loss difference and difference the Max.VUF, which revealed a high impact of the unbalanced system, connected the FCS to the RDS. The effect of the difference of maximum VUF (Diff. Max.VUF) was lower than the difference power loss (Diff. Power Loss).

Significantly, the high penetration of the FCS of the case 3C revealed as the total system loss had more effect than the percentage of the VUF. Therefore, the FCS is needed to provide in a three-phase system to reduce the unbalanced system. Moreover, the sizing and location of the FCS are significant to control and select in the optimal condition for lowering the power system loss.

4. CONCLUSSION

This paper succeeded in analyzing the impact of voltage unbalance systems when a fast-charging station is connected to the grid. The FCS and traditional loads were defined based on VDL for installing each scenario on the power system. The percentage of VUF profiles and total power loss were used to compare the values between the base case and each scenario. The rate of VUF profiles and the total power loss revealed the impact level of each scenario on the RDS. The comparison results from the percentage difference of the total power loss and the percentage difference of the VUF presented that the influence of the total power loss had more effect on the grid than the VUF. The highest impact on the difference of the total power loss was obtained in case of 3C at 74.8265 % and the difference in the maximum of VUF was 17.1579 %. Therefore, the percentage of penetration level and the installed position of the FCS are pivotal points in controlling and managing an optimal condition. However, the VUF factor is needed to analyze and improve the RDS together with the total power loss to enhance the power system stability in terms of voltage profiles under the VUF condition.

REFERENCES

[1] C. McFadden. (2018). A Brief History and Evolution of Electric Cars. Retrieved October 10, 2018 from the World Wide Web: https://interesting engineering.com/a-brief-history-and-evolution-of-electric-cars.

[2] IEA (2016), Global EV Outlook 2016: Beyond one million electric cars. Retrieved July 06, 2016 from the World Wide Web: https://doi.org/10.1787/ 9789264279469-en.

[3] S. Deb, K. Tammi, K. Kalita, and P. Mahanta, 2018. Impact of Electric Vehicle Charging Station Load on Distribution Network. Energies 11 (1): 1-25

[4] C. H. Dharmakeerthi, N. Mithulananthan, and T. K. Saha. 2014. Impact of electric vehicle fast charging on power system voltage stability. International Journal of Electrical Power & Energy Systems. 57: 241-249

[5] Y. Kongjeen and K. Bhumkittipich. 2016. Modeling of electric vehicle loads for power flow analysis based on PSAT. International Conference on Electrical Engineering/Electronics, Computer, Telecommunications and Information Technology (ECTI-CON). Chiang Mai, Thailand 28 June-1 July. DOI: 10.1109/ECTICon.2016.7561430

[6] M. Yilmaz and P. T. Krein. 2013. Review of Battery Charger Topologies, Charging Power Levels, and Infrastructure for Plug-In Electric and Hybrid Vehicles. IEEE Transactions on Power Electronics. 28 (5): 2151-2169.

[7] S. B. S. D. T. DemirokErhan ; Kjær, Remus. 2012. Three-Phase Unbalanced Load Flow Tool for Distribution Networks. in the 2nd International Workshop on Integration of Solar Power Systems, Energynautics GmbH. Lisbon, Portugal, 13-15 November.

[8] Y. Kongjeen, K. Bhumkittipich, N. Mithulananthan, I. S. Amiri, and P. Yupapin. 2019. A modified backward and forward sweep method for microgrid load flow analysis under different electric vehicle load mathematical models. Electric Power Systems Research, 168: 46-54.

[9] S. L. SANJUAN. 2010. Voltage Oriented Control of Three-Phase Boost PWM Converters Design, simulation and implementation of a 3- phase boost batterycharger. Master of Science Thesis in Electric Power Engineering, Department of Electric Power Engineering, Chalmers University of Technology, Göteborg, Sweden.

[10] Y.Kongjeen, K. Bhumkittipich and N. Mithulananthan. 2019. Optimal DG Sizing and Location in Modern Power Grids using PEVs Load Demand Probability. ECTI Transactions on Electrical Engineering, Electronics and Communications. 17 (1): pp. 51-59.

[11] IEC 61000-4-2. 2008. Electromagnetic compatibility (EMC)-Part 4-2: Testing and measurement techniques-Electrostatic discharge immunity test. Edition 2.0.

[12] IEEE std 1250^{TM}-2011. 2011. IEEE Guide for indentifying and improving Voltage Quality in Power Systems. Transmission and Distribution Committee of the IEEE Power & Energy Society. July 25.

[13] IEEE Std 241-1990. 1991. IEEE Recommended Practice for Electric Power Systems in Commercial Buildings. American National Standards Institute. May 17.

[14] IEEE Std 1159 ^{TM}-2009. 2009. IEEE Recommended Practice for Monitoring Electric Power Quality. IEEE Power & Energy Society. June 26.

[15] NEMA Standards Publication MG 1-2009. 2009. Motors and Generators. National Electrical manufacturers Association.

[16] Q. Ma and L. Xiao. (2017). Prediction model of BP neural network based on improved genetic algorithm optimization for infectious diseases. Chinese Automation Congress (CAC) Jinan, China 20-22 October. DOI: 10.1109/CAC.2017.8243521.